Nano Express

Broadband nanoplasmonic photodetector fabricated in ambient condition

To cite this article before publication: Debika Banerjee *et al* 2022 *Nano Ex.* in press https://doi.org/10.1088/2632-959X/aca2c8

Broadband nanoplasmonic photodetector fabricated in ambient condition

Debika Banerjee[1a], Ivy Asuo[1, 2, a], François-Xavier Fortier[1], Alain Pignolet[2], and Sylvain G. Cloutier[1*]

[1]*Dept. of Electrical Engineering, École de Technologie Supérieure, 1100 Notre-Dame Ouest, Montréal, QC, H3C 1K3Canada*

[2]*Institut National de la Recherche Scientifique (INRS), Énergie Matériaux Télécommunications Research Centre, 1650 Boul. Lionel Boulet, Varennes (QC), J3X 1S2, Canada*

[a]*Authors contributed equally*

** Address correspondence to sylvaing.cloutier@etsmtl.ca.*

Abstract: Surface plasmon are widely used to promote the exciton generation and light absorption in solar cells and photodetectors. In this work, a feasible approach for UV-VIS-NIR photodetection using plasmon-enhanced silicon nanowires (SiNWs) and amorphous TiO_2 heterostructure is presented. The photodetector shows excellent photo response up to 3.3 orders of magnitude enhancement with rise/decay times of 77/51 µs. Under small external bias (1V), the photodetector exhibits very high responsivity up to 49 A/W over a broadband wavelength range from 300-1100 nm. All the experimental procedures are performed at room temperature in ambient conditions. Its simple fabrication route and excellent performance make this photodetector distinct from similar architectures. Our finding offers new opportunities to engineer plasmon-based nanostructures in chemical sensors, optoelectronics and nanophotonic devices and applications.

Keywords: Silicon nanostructure, plasmonic effect, TiO_2, UV-VIS-NIR photodetectors, heterojunction.

1. Introduction

Nanoplasmonics has gained lots of attention thanks to its unique capability of light manipulation in the sub-wavelength regions[1-4]. From the historical Lycurgus cup[5], crafted by the Romans in 400 A.D., which consists of gold and silver nanoparticles suspended in glass to cutting edge devices like nanoscale laser, optical and photonic devices, biomedical imaging, and energy storage, it has a wide variety of applications[6-10]. Plasmonics technology can also be used to improve absorption in solar cells. As a result, solar photovoltaic absorber layers can be made considerably thinner, giving new design options for solar cells[4]. Photodetectors play a crucial role in photonic chips. The next generation of highly integrated photonic chips will require photodetectors with sub-nanometer details[11]. In recent years, researchers have achieved nanosecond response times with hybrid perovskite photodetectors[12]. The device architecture, however, is somewhat complex.

Plasmonic nanoparticles have unprecedented optical properties which further enhance the performance of the devices for various applications such as chemical sensing[13], detection, night vision, and spectroscopy[14]. Plasmon-enhanced nanostructures have been used for more than a decade now to fabricate high performance photodetectors. The preparation process, however, is usually complicated and expensive because mostly electron beam lithography is utilized to prepare the nanostructures[15]. Other than that, several chemical and physical techniques are used to synthesize the plasmonic nanoparticles such as seed induced nucleation, ion exchange methods, galvanic displacement methods etc.[16-18]. Seed mediated nucleation relies on the degree of the lattice matching between different components which are challenging to achieve. Yet these plasmon-enhanced nanostructured devices still required high bias voltages, high temperatures, or other complex fabrication processes in order to perform as desired[3]. In contrast, galvanic displacement uses all solution-based chemical redox reactions in which metallic nanoparticles are reduced, deposited, and the substrate is oxidized. This technique offers precise control over the nanostructure's length, diameter, and other important parameters[18-20].

During the past two decades, Silicon nanowires (SiNWs) have gained considerable attention due to their unique chemical and physical properties[21-24]. The confluence of the confinement of one-dimensional nanostructure with the plasmonic effect of metallic nanoparticles makes the best use of the SiNWs in sub nano dimensions. The surface functionalization of SiNWs using Ag nanoparticles enhances the UV to NIR absorption through the nanoplasmonic effect, collecting and transporting the photo excited electrons to the electrodes[25, 26].

Crystalline TiO_2 gained much attention for its metal-oxide-semiconductor nature since decades. The large band gap of TiO_2 makes it a suitable material for UV detection[27-30]. The amorphous phase of TiO_2 has not been explored as extensively before, despite of having similar electronic properties as the crystalline phase[31, 32]. We have previously optimized amorphous TiO_2 based photodetectors to have similar behavior, which is comparable to anatase TiO_2 based devices[33, 34]. Making a heterojunction with amorphous TiO_2 in conjunction with plasmonic SiNWs extends its detection ability in a broadband wavelength range from UV to NIR.

To address the current problems regarding broadband photodetection using low bias, simple fabrication route and good performances, we have demonstrated a photodetector architecture using plasmon sensitized n-SiNWs / amorphous TiO_2 heterostructure in this manuscript. When exposed to air, SiNWs form native oxide layer. The native oxide layer acts as an electrical insulator, further limiting the conduction across the junction of the device[35]. Adding TiO_2 on top of SiNWs to form the heterojunction enhances device performance by reducing electron injection barriers and enabling a larger electron flow[36]. TiO_2 is reported to have a greater thermodynamic stability than SiO_2 in the literature[37].The geometry of the SiNWs enhances with the Ag nanoparticles which further increase the UV and NIR absorption through the nanoplasmonic effect. Similar architecture shows excellent photoelectrochemical performance indicating its application across various fields[38]. The device fabrication process, however, was more complex than the current research.

2. Results and discussions

Plasmon sensitized SiNWs are fabricated using galvanic displacement method (GDM). The details of the synthesis process are described in the materials and method section. Figure 1a shows the surface morphology of the as synthesized plasmon sensitized SiNWs. The 45^0 tilted

cross-sectional SEM image is depicted in the figure 1b. Commercially available amorphous TiO_2 sol-gel are spin coated on top of the plasmon sensitized SiNWs. The surface and 45^0 tilted cross-sectional SEM images of the heterojunction are depicted in the figure 1c and 1d respectively. The plasmonic nanowires structure on Si substrate contributes to generating more electron hole pairs (EHPs) by trapping more of the incident light. As suggested by the literature[2, 39, 40], the nanoplasmonic SiNWs have increased scattering cross-section and optical path length which further helps in light harvesting and light trapping. As a result, these nanoplasmonic SiNWs produces more EHPs. The UV/VIS/NIR spectroscopic plot in figure 2a reveals the enhanced near UV and NIR absorption of the nanoplasmonic SiNWs to benefit the creation of EHPs.

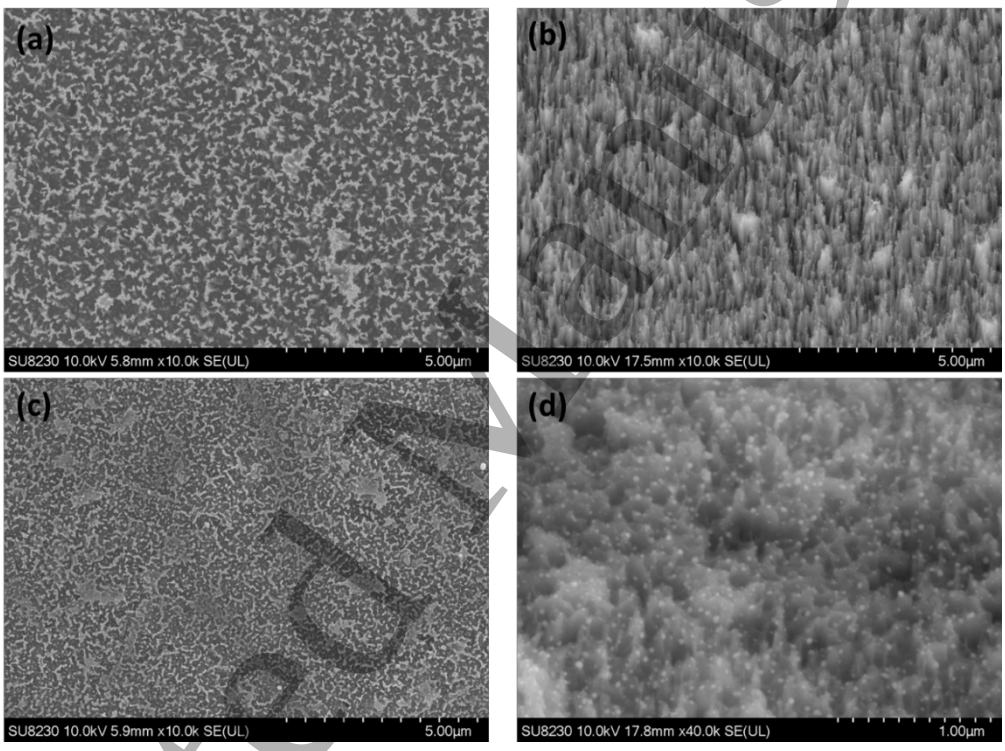

Figure 1: (a) Surface, and (b) 45^0 tilted SEM images of the plasmon induced SiNWs, (c) Surface, and (d) 45^0 tilted SEM images of the plasmon induced SiNWs/amorphous TiO_2 heterojunction.

Aiming at increasing optical absorption in nanoplasmonic SiNWs, the volumetric proportion of Ag nanoparticles is controlled by the cleaning process after GDM. The big dendrite layers of Ag are removed using dilute HNO_3 leaving the minute amounts of Ag nanoparticles on the top and the sidewalls of the SiNWs. The reduced reflection of the nanoplasmonic SiNWs after removing the dendrite layers can be attributed to the increased absorption due to a strong interaction between the free electrons in the Ag nanoparticles and the incident electromagnetic radiation. However, the nanoplasmonic SiNWs with the dendrite layers (before cleaning) results in increased reflection (shown in the figure S1 in the supplementary information section) as the larger density of Ag leads to the percolation effect[41], hence acquiring a strong metallic character that inhibits refraction into the layer. In addition to the reflection spectrum of SiNWs, it is evident that the addition of nanoplasmonic Ag results a remarkable reduction of the reflection. This behavior can be ascribed to the higher imaginary

value of the refractive index that further contributes to the increased optical absorption by the Ag nanoparticles. Moreover, the maxima and minima values of reflectance are getting shifted due to the changes of the complex nature of the effective refractive index in the spectrum. This effect can be attributed to GDM which deposits Ag nanoparticles and creates pores as well. The nanoplasmonic Ag suppress the reflectance from the SiNWs throughout the entire polychromatic spectrum. The reflectance reduction from the UV region can be attributed to the quadrupolar resonance effect of Ag nanoparticles[42, 43]. Scattering of light takes place due to the large distribution (from 5-100 nm) of the nanoparticle sizes. Figure 2c demonstrates the size distribution of the Ag nanoparticles from the SEM image (figure 2b) using image J freeware. The nanoparticles are varied between 5 nm size up to 100 nm. When the nanoparticle size is <20 nm, the forward scattering increases due to the small contact area between the nanoplasmons and nanowires which establishes a good agreement with the literature[44, 45]. The reduction of reflectance from the VIS and NIR region is due to the increased Ag nanoparticle size which provides greater surface coverage on SiNWs[42]. Near the band gap, Si cannot absorb much light. Therefore, even a small reflection reduction is very significant near the band gap region.

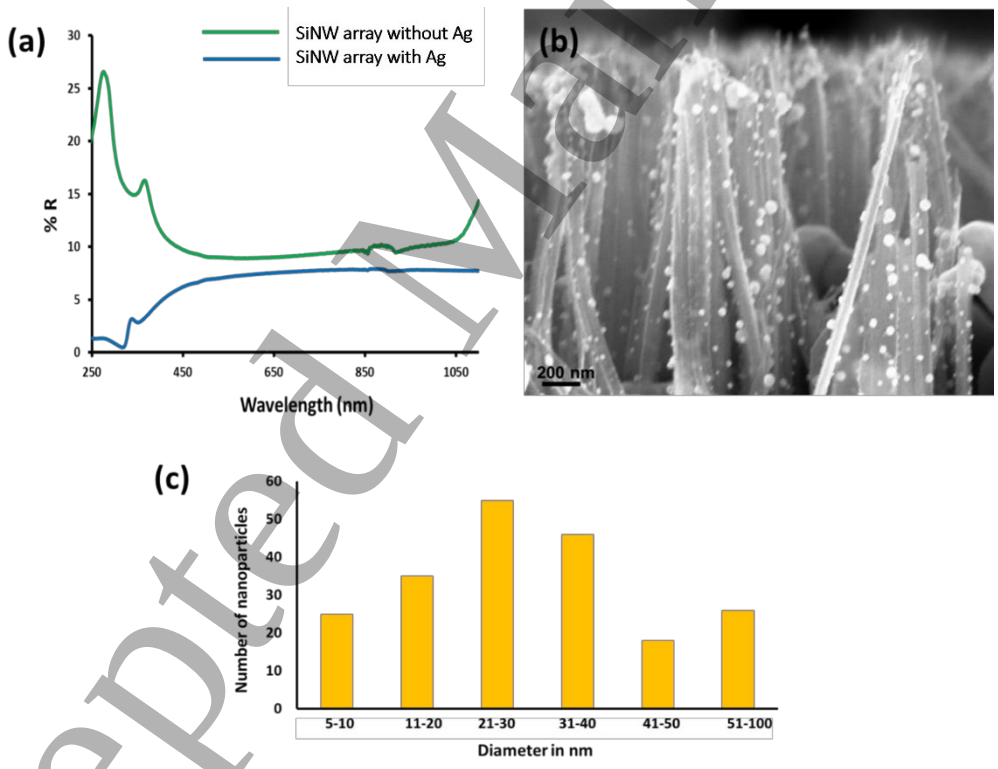

Figure 2: (a) Optical reflectance of SiNWs arrays and nanoplasmonic SiNWs arrays, (b) Nanoplasmonic SiNWs, and (c) Ag nanoparticle size distribution

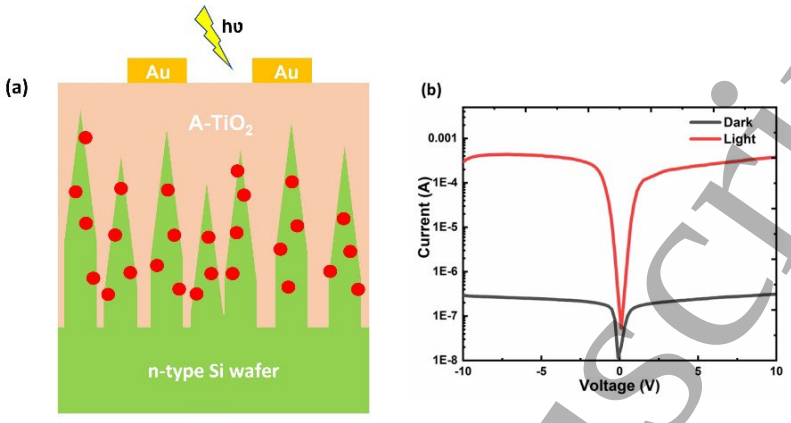

Figure 3: (a) Device architecture and (b) Current vs. voltage characteristics of the plasmon induced SiNWs/amorphous TiO_2 heterojunction photodetector.

The schematic of the photodetector device has been illustrated in figure 3a. The photo response properties of the photodetector are demonstrated by the current vs. voltage characteristic in the dark and 1.5 G illumination as shown in figure 3b. It clearly shows that the current of the device increases significantly up to 3.3 orders upon illumination with A.M. 1.5 G incident light at room temperature.

Due to having a wide bandgap of around 3.2 eV, TiO_2 produces photo generated carriers under 1V applied bias and UV illumination. Similarly, the nanoplasmonic SiNWs produced photo generated carriers under 1V applied bias and near UV-VIS-NIR illumination thanks to the plasmonic effect and relatively narrow band gap of Si. Surface plasmons can trigger plasmonic hot carriers with higher energy than those induced by direct excitations. SiNWs have a wider band gap than bulk Si because of the nanostructure. Researchers have found that SiNWs have a broad absorption spectrum, which is a consequence of bandgap broadening compared to bulk material[46]. Using the Kubelka-Monk method[47], S. D. Hutagalung and his team calculated the bandgap of MACE synthesized SiNWs in 2017 and determined that their bandgap is little wider (1.2 eV) as compared to their bulk counterparts (1.12 eV at room temperature)[46], and validated their results through other literature[48, 49]. Since the Fermi level of the SiNWs is higher than the Si substrate, electrons will flow from SiNWs to Si and a depletion region will be formed in SiNWs region. The band diagram of the photodetector device is shown in figure 4.

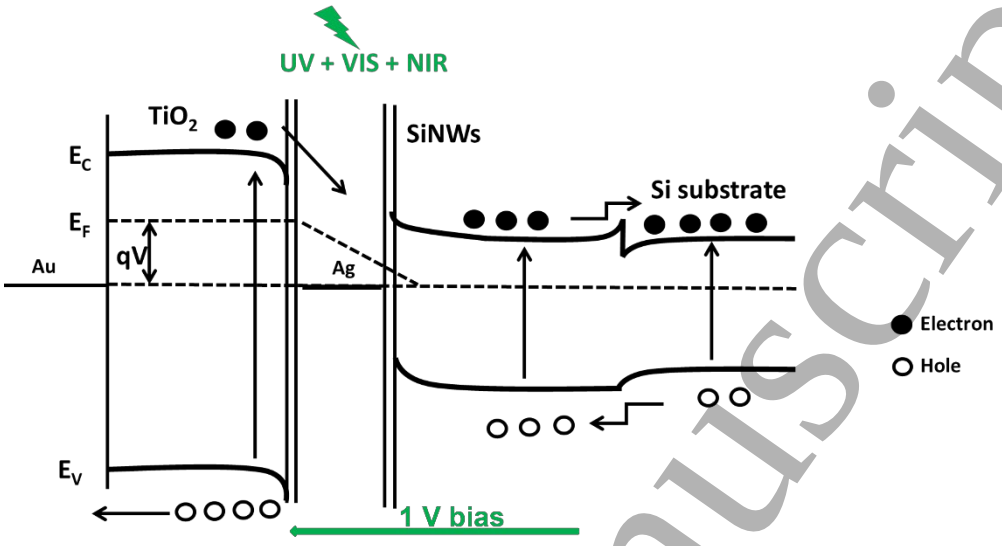

Figure 4: Band diagram of the charge separation process under 1V external bias.

The transient photo response behavior of the photodetector device is analyzed as demonstrated in the figure 5a and 5b. The response times of the photodetectors are determined by the rise and the decay times using a bi-exponential curve fitting as shown in figure S3 in the supplementary document section which is a method reported in the literature[50-52].

The rise and decay times of the photodetector device are found to be 77 µs and 51 µs respectively which indicates the fast response behavior from the nanoplasmonic photodetector devices. The small rise/decay times assure relatively fast response detection for several applications like portable equipment considering such a simple route of fabrication.

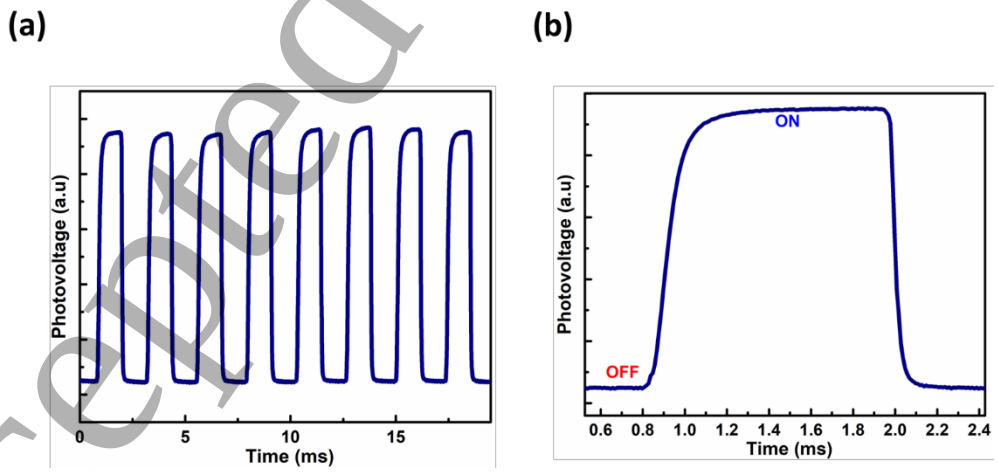

Figure 5: (a) Transient photo response of the plasmon induced SiNWs/amorphous TiO_2 heterojunction, (b) A single pulse from (a) use for the determination of the rise and decay of the current in time through bi-exponential fitting.

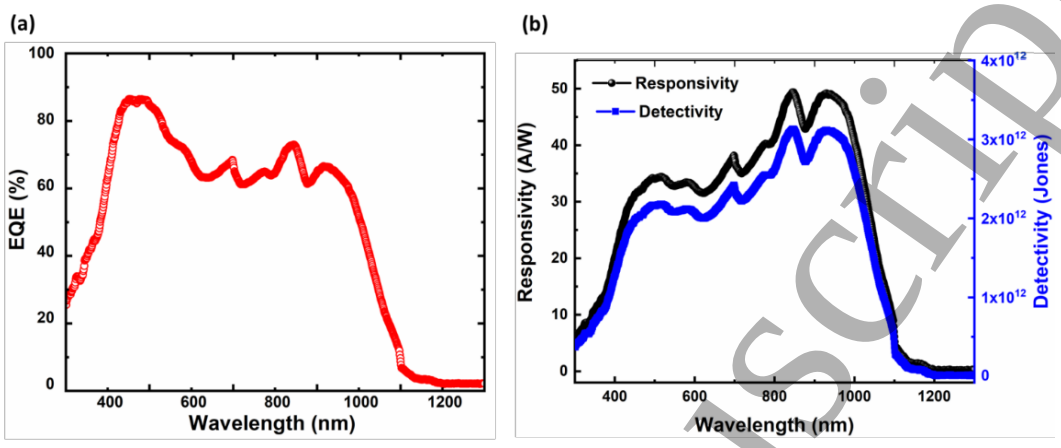

Figure 6: (a) EQE and (b) Responsivity and detectivity plot of the plasmon induced SiNWs/amorphous TiO_2 heterojunction.

To complete the evaluation of the nanoplasmonic photodetector devices, the external quantum efficiency, responsivity and detectivity of the devices are probed using 1V external bias. Figure 6a shows the EQE in a broadband wavelength range from 300-1100 nm. The peak value of the EQE reaches up to 85% at 475 nm. Another crucial parameter is the spectral responsivity which determines the spectral behavior of the photodetectors. The spectral responsivity is characterized by the method described in the materials and method section and used the formula: $D^* = R(A)^{1/2}/(2eI_d)^{1/2}$ to calculate the detectivity (where A denotes the active area (0.009 cm^2) of the device, R is the responsivity, I_d is the dark current, and e is the elementary charge). Figure 6b illustrates the spectral responsivity and detectivity of the nanoplasmonic photodetector device from 300-1100 wavelength range under 1 V external bias. The peak responsivity reaches up to 11 A/W in the near UV region, and 34 A/W and 49 A/W in the VIS and NIR region respectively. The detectivity of these photodetector devices reaches up to 6.84 E^{11} Jones, 2.16 E^{12} Jones and 3.11 E^{12} Jones in the near UV, VIS and NIR regions respectively. Simply adding these minute amounts of Ag nanoparticles extends the photodetection from UV-VIS region to UV-VIS-NIR region as compared to the pristine SiNWs/ amorphous TiO_2 devices as shown in our previous report[33]. Table 1 illustrates the performance comparison between the pristine and nanoplasmonic SiNWs/ amorphous TiO_2 based photodetectors. Hence, the superior performance of the nanoplasmonic photodetector as compared to our previous report[33] can be attributed to the nanoplasmonic effect. If the photon energy is too low while the wavelength is very long, then the essential condition for the bandgap ($hv > E_g$, where hv is the photon energy and E_g is the bandgap) no longer holds, causing the responsivity to drop to zero. Indeed, we can see significantly higher responsivity values (figure 6b) in the NIR region as compared to the VIS and UV region. The peak values of responsivity, EQE and detectivity at different wavelengths of the nanoplasmonic photodetector are illustrated in the table 2.

Table 1: Performance comparison between pristine[33] and nanoplasmonic SiNWs/amorphous TiO_2 photodetectors.

Wavelength (nm)	EQE (%)	R (A/W)	Rise/Decay times	Dark to Photocurrent enhancement ratio
350	25 (pristine) 38 (nanoplasmonic)	6 (pristine) 11 (nanoplasmonic)	0.23/0.17ms (pristine) 77/51 µs (nanoplasmonic)	2 orders of magnitude (pristine) 3.3 orders of magnitude (nanoplasmonic)
500	76 (pristine) 84 (nanoplasmonic)	25 (pristine) 34 (nanoplasmonic)		
1000	N/A (pristine) 50 (nanoplasmonic)	N/A (pristine) 41 (nanoplasmonic)		

Table 2: EQE, responsivity and detectivity values at different wavelengths (near UV, VIS, NIR).

Wavelength (nm)	EQE (%)	R (A/W)	D* (Jones)
350	38.18	10.78	6.84 E ^{11}
500	84.29	34.04	2.16 E ^{12}
1000	50.35	40.65	2.58 E ^{12}
Maximum/peak values	85.88 at 475 nm	49.16 at 930 nm	3.11 E ^{12} at 930 nm

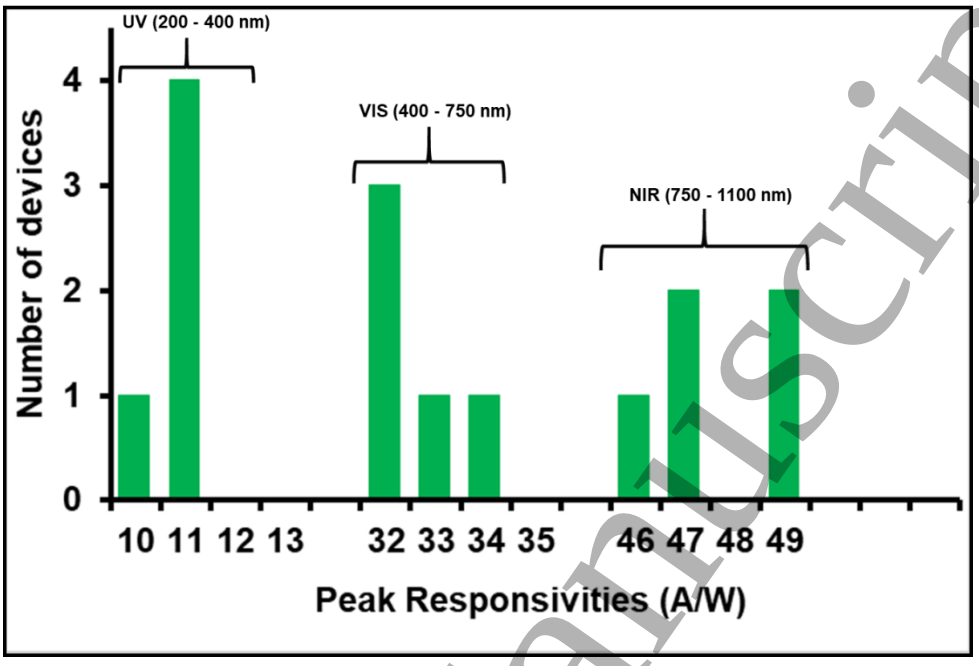

Figure 7: Histogram of the responsivity in the UV, VIS and NIR region for 5 photodetectors.

Figure 7 illustrates the histogram of the peak values of the responsivities of 5 photodetector devices. In the near UV region, the photodetector devices demonstrate peak responsivities between 10-11 A/W, in the VIS region, the responsivities lie between 32-34 A/W, while in the NIR region the peak value of the responsivity lies in the range of 46-49 A/W. The histogram discloses good reproducibility and superior performances for all the photodetector devices.

Table 3 demonstrates the performance comparison of the photodetector devices with the state-of-the-art devices. With a low applied bias (1V), this work reports a fast UV/VIS/NIR photodetector with high responsivities. Since it relies completely on solution-based fabrication under ambient conditions, it is also the most accessible of alternative fabrication methods.

Table 3: Comparison of the key parameters with the state-of-the-art.

Paper	Rise/decay times	Responsivity	External bias	Processing temperature	Morphology	Method
Selman *et.al.*[53], 2015	50.8/57.8 ms	0.45 A/W @ 325 nm	5V	550 C	p-Si/rutile TiO_2 nanorod	sputtering
Hosseini *et.al.[54]*, 2016	60/150 s	N/A	4.2V	850 C	p-Si/n-TiO_2 nanostructures	Thermal oxidation growth
Ji *et.al.*[28] 2017	0.05/0.05 s	17 mA/W @365 nm, 2	-2 to -4V	600 C	n-Si/TiO_2 nanorod	Sputtering

		A/W @565 nm				
Banerjee *et.al*.[33] 2019 (previous work)	0.23/0.17 ms	6 A/W @ 350 nm, 25 A/W @ 500 nm	1V	Room temperature	n-SiNWs/amorphous TiO_2 thin film	All solution based
Banerjee *et.al*.[34] 2020 (previous work)	0.16/0.14 ms	10 A/W @ 350 nm, 33 A/W @ 500 nm	1V	Room temperature	n-porous Si/amorphous TiO_2 thin film	All solution based
El-Mahalawy *et.al*.[11] 2022	50.2/52.8 ms	70.8 mA/W @ 280 nm	Self powered	60 C	Plasmonic n-TiO_2/p-Si	All solution based
Banerjee *et.al.* 2022 (this work)	77/51 µs	11 A/W @ 350 nm, 34 A/W @ 500 nm, 41 A/W @ 1000 nm	1V	Room temperature	Nanoplasmonic n-SiNWs/amorphous TiO_2 thin film	All solution based

3. Materials and methods

3.1 Fabrication procedure

Plasmon sensitized SiNWs are fabricated by employing all solution based GDM. Details of the GDM have been described elsewhere[55, 56]. For this study, we have used low doped n type Si wafer with the resistivity of 1-10 ohm-cm. The etchant solution contains 0.02M silver nitrate ($AgNO_3$) solution and 4.6M hydrogen fluoride (HF) solution mixed in 1:1 ratio. The Si substrates have cleaved into 1 cm^2 pieces and cleaned using ultra sonication with acetone and IPA for 15 minutes each. Then the Si pieces have rinsed with deionized (DI) water and dried using nitrogen (N_2) flow. The cleaned samples are transferred immediately into the etching bath at room temperature for 40 minutes. After the etching, vertically aligned SiNWs have been formed covered with Ag dendrites layers. These Ag dendrites layers are removed using diluted nitric acid (HNO_3) solution (1:5 of 70% HNO_3 and DI water) for 30 minutes at room temperature. Vertically aligned SiNWs with Ag nanoparticles on the sidewalls of the nanowires are found after the cleaning. Pure SiNWs have found without any Ag contamination when the cleaning has been done using concentrated (70%) HNO_3 at room temperature for 1 hour. Hence, the post cleaning protocol after the fabrication of the nanowires plays the key role to achieve plasmon sensitized SiNWs. These nanowires vary from 800-1000nm in length and 40-50 nm in diameter. The etching takes place in the laboratory environment with 40% humidity at room temperature. Then, a thin film layer (~120 nm) of amorphous TiO_2 sol-gel purchased from Solaronix is deposited using spin-coating technique to form the heterojunction. Finally, 50µm channels of gold pads are evaporated atop the heterojunction photodetector.

3.2 Materials and device characterizations

The morphology of nanoplasmonic SiNWs and TiO_2 thin films are probed using a Hitachi SU30 scanning electron microscope (SEM). The reflectance measurements are performed using Perkin Elmer LAMBDA 750 UV/VIS system. A Keithley 2400 source measuring unit (SMU) equipped with a Newport solar simulator is used to characterize the current-voltage behavior of the photodetector device.

Xenon lamp and TRIAX320 monochromator are used for spectral responsivity measurements as previously described[50, 57]. A 10 nm-step scan from 300 to 1100 nm is performed using the light from the Xenon lamp first passing through a monochromator. A modulation at 100 Hz is applied to the excitation light before the sample is illuminated. An external bias of 1 V is applied to the sample, which is placed before a circular diaphragm. In the final step, a lock-in amplifier is used to measure the photocurrent. Using a calibrated photodiode (Newport 918D) placed at the same diaphragm aperture as the sample, we calculate the responsivity by dividing the photocurrent by the power of the incident light at each wavelength. The spectral plot is used to extract the responsivity at certain wavelengths.

The transient behavior of the photoresponse is characterized with a continuous illumination from a 532 nm laser of power density of the laser is 0.5 $mW.mm^{-2}$ and Agilent DSO-X 3034 A oscilloscope via a 1 GΩ load resistance as previously reported[57]. The measurements are all performed at room temperature.

4. Conclusions

To conclude, we have experimentally illustrated improved UV/VIS/NIR photodetection from chemically synthesized nanoplasmonic heterostructure. Peak performances reach 49 A/W, 85% EQE and 77/51 µs rise/decay times. Moreover, these, devices allow operation over a broad spectrum with performances exceeding 10 A/W and 30% EQE from 300 nm to 1100 nm. The superior detectivity can be helpful in the detection of weak optical signals. These all-solution-based syntheses of nanoplasmonic heterostructures have the potential to reduce the cost of future nanoengineered devices.

Acknowledgements. S.G.C. is thankful to the NSERC Discovery Program, Canada Research Chairs program and FRQNT-Team program for financial support. I.M.A. is thankful to the MATECSS and FRQNT fellowships for financial support.

Disclosures. The authors declare no conflicts of interest.

Data availability. Data underlying the results presented in this paper are not publicly available at this time but may be obtained from the authors upon reasonable request.

See supplementary document for supporting content.

References

[1] K.-T. Lin, H. Lin, and B. Jia, "Plasmonic nanostructures in photodetection, energy conversion and beyond," *Nanophotonics,* vol. 9, no. 10, pp. 3135-3163, 2020, doi: doi:10.1515/nanoph-2020-0104.

[2] D. Banerjee, X. Guo, and S. G. Cloutier, "Plasmon-Enhanced Silicon Nanowire Array-Based Hybrid Heterojunction Solar Cells," *Solar RRL,* vol. 0, no. 0, p. 1800007, doi: doi:10.1002/solr.201800007.

[3] A. Philip and A. R. Kumar, "The performance enhancement of surface plasmon resonance optical sensors using nanomaterials: A review," *Coordination Chemistry Reviews,* vol. 458, p. 214424, 2022/05/01/ 2022, doi: https://doi.org/10.1016/j.ccr.2022.214424.

[4] H. A. Atwater and A. Polman, "Plasmonics for improved photovoltaic devices," *Nature Materials,* vol. 9, no. 3, pp. 205-213, 2010/03/01 2010, doi: 10.1038/nmat2629.

[5] I. Freestone, N. Meeks, M. Sax, and C. Higgitt, "The Lycurgus Cup — A Roman nanotechnology," *Gold Bulletin,* vol. 40, no. 4, pp. 270-277, 2007/12/01 2007, doi: 10.1007/BF03215599.

[6] A. Yang *et al.*, "Real-time tunable lasing from plasmonic nanocavity arrays," *Nature Communications,* vol. 6, no. 1, p. 6939, 2015/04/20 2015, doi: 10.1038/ncomms7939.

[7] M. Heo, H. Cho, J.-W. Jung, J.-R. Jeong, S. Park, and J. Y. Kim, "High-Performance Organic Optoelectronic Devices Enhanced by Surface Plasmon Resonance," *Advanced Materials,* vol. 23, no. 47, pp. 5689-5693, 2011, doi: https://doi.org/10.1002/adma.201103753.

[8] Z. Liang, J. Sun, Y. Jiang, L. Jiang, and X. Chen, "Plasmonic Enhanced Optoelectronic Devices," *Plasmonics,* vol. 9, no. 4, pp. 859-866, 2014/08/01 2014, doi: 10.1007/s11468-014-9682-7.

[9] J. Zeng *et al.*, "Direct Synthesis of Water-Dispersible Magnetic/Plasmonic Heteronanostructures for Multimodality Biomedical Imaging," *Nano Letters,* vol. 19, no. 5, pp. 3011-3018, 2019/05/08 2019, doi: 10.1021/acs.nanolett.9b00171.

[10] A. B. Bucharskaya *et al.*, "Photothermal and Photodynamic Therapy of Tumors with Plasmonic Nanoparticles: Challenges and Prospects," *Materials,* vol. 15, no. 4, p. 1606, 2022. [Online]. Available: https://www.mdpi.com/1996-1944/15/4/1606.

[11] A. M. El-Mahalawy, M. M. Abdrabou, A. R. Wassel, M. A. El-Salam, and F. M. Amin, "Plasmonic enhanced ultraviolet photodetection performance of n-TiO2/p-Si anisotype heterojunction with aluminum patterned array," *Journal of Physics and Chemistry of Solids,* vol. 170, p. 110943, 2022/11/01/ 2022, doi: https://doi.org/10.1016/j.jpcs.2022.110943.

[12] C. Li *et al.*, "Ultrafast and broadband photodetectors based on a perovskite/organic bulk heterojunction for large-dynamic-range imaging," *Light: Science & Applications,* vol. 9, no. 1, p. 31, 2020/03/03 2020, doi: 10.1038/s41377-020-0264-5.

[13] N. H. Ly, H. H. Kim, and S.-W. Joo, "On-Site Detection for Hazardous Materials in Chemical Accidents," *Bulletin of the Korean Chemical Society,* vol. 42, no. 1, pp. 4-16, 2021, doi: https://doi.org/10.1002/bkcs.12140.

[14] D. K. Gramotnev and S. I. Bozhevolnyi, "Plasmonics beyond the diffraction limit," *Nature Photonics,* vol. 4, no. 2, pp. 83-91, 2010/02/01 2010, doi: 10.1038/nphoton.2009.282.

[15] M. Freitag, T. Low, W. Zhu, H. Yan, F. Xia, and P. Avouris, "Photocurrent in graphene harnessed by tunable intrinsic plasmons," *Nature Communications,* vol. 4, no. 1, p. 1951, 2013/06/03 2013, doi: 10.1038/ncomms2951.

[16] G. Zheng, S. Mourdikoudis, and Z. Zhang, "Plasmonic Metallic Heteromeric Nanostructures," *Small,* vol. 16, no. 38, p. 2002588, 2020, doi: https://doi.org/10.1002/smll.202002588.

[17] S. Zhang, J. Li, X. Wang, Y. Huang, M. Zeng, and J. Xu, "In Situ Ion Exchange Synthesis of Strongly Coupled Ag@AgCl/g-C3N4 Porous Nanosheets as Plasmonic Photocatalyst for Highly Efficient Visible-Light Photocatalysis," *ACS Applied Materials & Interfaces,* vol. 6, no. 24, pp. 22116-22125, 2014/12/24 2014, doi: 10.1021/am505528c.

[18] Y. S. Yamamoto, Y. Fujime, N. Takahashi, S. Nakanishi, and T. Itoh, "Formation mechanism of plasmonic silver nanohexagonal particles made by galvanic displacement reaction," *RSC Advances,* 10.1039/C6RA00685J vol. 6, no. 37, pp. 31454-31461, 2016, doi: 10.1039/C6RA00685J.

[19] L. Magagnin, R. Maboudian, and C. Carraro, "Gold Deposition by Galvanic Displacement on Semiconductor Surfaces: Effect of Substrate on Adhesion," *The Journal of Physical Chemistry B,* vol. 106, no. 2, pp. 401-407, 2002/01/01 2002, doi: 10.1021/jp013396p.

[20] H. Kawasaki *et al.*, "Platinum nanoflowers on scratched silicon by galvanic displacement for an effective SALDI substrate," (in eng), *Chemistry (Weinheim an der Bergstrasse, Germany),* vol. 16, no. 35, pp. 10832-43, Sep 17 2010, doi: 10.1002/chem.201001038.

[21] K. Q. Peng *et al.*, "Fabrication of Single-Crystalline Silicon Nanowires by Scratching a Silicon Surface with Catalytic Metal Particles," *Advanced Functional Materials,* vol. 16, no. 3, pp. 387-394, 2006, doi: 10.1002/adfm.200500392.

[22] V. Schmidt, J. V. Wittemann, S. Senz, and U. Gösele, "Silicon Nanowires: A Review on Aspects of their Growth and their Electrical Properties," *Advanced Materials,* vol. 21, no. 25-26, pp. 2681-2702, 2009, doi: 10.1002/adma.200803754.

[23] G. Collins and J. D. Holmes, "Chemical functionalisation of silicon and germanium nanowires," *Journal of Materials Chemistry,* 10.1039/C1JM11028D vol. 21, no. 30, pp. 11052-11069, 2011, doi: 10.1039/C1JM11028D.

[24] A. Mohamedyaseen and P. S. Kumar, "The Fabrication of High-Anisotropy Silicon Nanowires Based on MACE Method for Photonic Sensor," *Silicon,* 2022/04/11 2022, doi: 10.1007/s12633-022-01751-2.

[25] E. Garnett and P. Yang, "Light Trapping in Silicon Nanowire Solar Cells," *Nano Letters,* vol. 10, no. 3, pp. 1082-1087, 2010/03/10 2010, doi: 10.1021/nl100161z.

[26] B. Y. Huang *et al.*, "Solution-processed silicon hybrid heterojunction photovoltaics with silver nanowires," in *2012 38th IEEE Photovoltaic Specialists Conference*, 3-8 June 2012 2012, pp. 002537-002539, doi: 10.1109/PVSC.2012.6318111.

[27] J. Zou, Q. Zhang, K. Huang, and N. Marzari, "Ultraviolet Photodetectors Based on Anodic TiO2 Nanotube Arrays," *The Journal of Physical Chemistry C,* vol. 114, no. 24, pp. 10725-10729, 2010/06/24 2010, doi: 10.1021/jp1011236.

[28] T. Ji *et al.*, "Enhanced UV-visible light photodetectors with a TiO2/Si heterojunction using band engineering," *Journal of Materials Chemistry C,* 10.1039/C7TC04811D vol. 5, no. 48, pp. 12848-12856, 2017, doi: 10.1039/C7TC04811D.

[29] H. Chong *et al.*, "High-performance solar-blind ultraviolet photodetector based on electrospun TiO2-ZnTiO3 heterojunction nanowires," *Nano Research,* journal article vol. 8, no. 9, pp. 2822-2832, September 01 2015, doi: 10.1007/s12274-015-0787-x.

[30] P. V. K. Yadav, B. Ajitha, C. M. A. Ahmed, Y. A. K. Reddy, and V. R. Minnam Reddy, "Superior UV photodetector performance of TiO2 films using Nb doping," *Journal of Physics and Chemistry of Solids,* vol. 160, p. 110350, 2022/01/01/ 2022, doi: https://doi.org/10.1016/j.jpcs.2021.110350.

[31] K. Kaur and C. V. Singh, "Amorphous TiO2 as a Photocatalyst for Hydrogen Production: A DFT Study of Structural and Electronic Properties," *Energy Procedia,*

vol. 29, pp. 291-299, 2012/01/01/ 2012, doi: https://doi.org/10.1016/j.egypro.2012.09.035.

[32] K. T. Selvi and S. Sagadevan, "2 - Recent developments in optoelectronic and photonic applications of metal oxides," in *Metal Oxides for Optoelectronics and Optics-Based Medical Applications*, S. Sagadevan, J. Podder, and F. Mohammad Eds.: Elsevier, 2022, pp. 33-57.

[33] D. Banerjee, I. M. Asuo, A. Pignolet, and S. G. Cloutier, "Low-cost photodetector architectures fabricated at room-temperature using nano-engineered silicon wafer and sol-gel TiO2 – based heterostructures," *Scientific Reports,* vol. 9, no. 1, p. 17994, 2019/11/29 2019, doi: 10.1038/s41598-019-54481-8.

[34] D. Banerjee, I. M. Asuo, A. Pignolet, R. Nechache, and S. G. Cloutier, "High performance photodetectors using porous silicon-TiO2 heterostructure," *Engineering Research Express,* vol. 2, no. 3, p. 035021, 2020/09/14 2020, doi: 10.1088/2631-8695/abb06d.

[35] K. Heo *et al.*, "Large-Scale Assembly of Silicon Nanowire Network-Based Devices Using Conventional Microfabrication Facilities," *Nano Letters,* vol. 8, no. 12, pp. 4523-4527, 2008/12/10 2008, doi: 10.1021/nl802570m.

[36] E. Memarzadeh Lotfabad *et al.*, "ALD TiO2 coated silicon nanowires for lithium ion battery anodes with enhanced cycling stability and coulombic efficiency," *Physical Chemistry Chemical Physics,* 10.1039/C3CP52485J vol. 15, no. 32, pp. 13646-13657, 2013, doi: 10.1039/C3CP52485J.

[37] L. Brewer, "Thermodynamic Properties of the Oxides and their Vaporization Processes," *Chemical Reviews,* vol. 52, no. 1, pp. 1-75, 1953/02/01 1953, doi: 10.1021/cr60161a001.

[38] X. Gao, S. Wu, J. Yan, X. Zhai, and X. Li, "Stabilized and Improved Photoelectrochemical Responses of Silicon Nanowires Modified with Ag@SiO(2) Nanoparticles and Crystallized TiO(2) Film," (in eng), *ACS Appl Mater Interfaces,* vol. 8, no. 44, pp. 30072-30078, Nov 9 2016, doi: 10.1021/acsami.6b06912.

[39] C. Fei Guo, T. Sun, F. Cao, Q. Liu, and Z. Ren, "Metallic nanostructures for light trapping in energy-harvesting devices," *Light: Science & Applications,* vol. 3, no. 4, pp. e161-e161, 2014/04/01 2014, doi: 10.1038/lsa.2014.42.

[40] S. Morawiec, M. J. Mendes, F. Priolo, and I. Crupi, "Plasmonic nanostructures for light trapping in thin-film solar cells," *Materials Science in Semiconductor Processing,* vol. 92, pp. 10-18, 2019/03/15/ 2019, doi: https://doi.org/10.1016/j.mssp.2018.04.035.

[41] S. De, P. J. King, P. E. Lyons, U. Khan, and J. N. Coleman, "Size Effects and the Problem with Percolation in Nanostructured Transparent Conductors," *ACS nano,* vol. 4, no. 12, pp. 7064-7072, 2010/12/28 2010, doi: 10.1021/nn1025803.

[42] E. Thouti, N. Chander, V. Dutta, and V. K. Komarala, "Optical properties of Ag nanoparticle layers deposited on silicon substrates," *Journal of Optics,* vol. 15, no. 3, p. 035005, 2013/02/27 2013, doi: 10.1088/2040-8978/15/3/035005.

[43] N. G. Bastús, J. Piella, and V. Puntes, "Quantifying the Sensitivity of Multipolar (Dipolar, Quadrupolar, and Octapolar) Surface Plasmon Resonances in Silver Nanoparticles: The Effect of Size, Composition, and Surface Coating," (in eng), *Langmuir,* vol. 32, no. 1, pp. 290-300, Jan 12 2016, doi: 10.1021/acs.langmuir.5b03859.

[44] H. Dai, M. Li, Y. Li, H. Yu, F. Bai, and X. Ren, "Effective light trapping enhancement by plasmonic Ag nanoparticles on silicon pyramid surface," *Opt. Express,* vol. 20, no. S4, pp. A502-A509, 2012/07/02 2012, doi: 10.1364/OE.20.00A502.

[45] M. Schmid, R. Klenk, M. Lux-Steiner, M. Topic, and J. Krc, "Modeling plasmonic scattering combined with thin-film optics," (in eng), *Nanotechnology,* vol. 22, no. 2, p. 025204, Jan 14 2011, doi: 10.1088/0957-4484/22/2/025204.

[46] S. D. Hutagalung, M. M. Fadhali, R. A. Areshi, and F. D. Tan, "Optical and Electrical Characteristics of Silicon Nanowires Prepared by Electroless Etching," *Nanoscale Research Letters,* vol. 12, no. 1, p. 425, 2017/06/24 2017, doi: 10.1186/s11671-017-2197-3.

[47] R. López and R. Gómez, "Band-gap energy estimation from diffuse reflectance measurements on sol–gel and commercial TiO2: a comparative study," *Journal of Sol-Gel Science and Technology,* vol. 61, no. 1, pp. 1-7, 2012/01/01 2012, doi: 10.1007/s10971-011-2582-9.

[48] Z. Huang, H. Fang, and J. Zhu, "Fabrication of Silicon Nanowire Arrays with Controlled Diameter, Length, and Density," *Advanced Materials,* vol. 19, no. 5, pp. 744-748, 2007, doi: https://doi.org/10.1002/adma.200600892.

[49] Y. Kurokawa, M. Yano, S. Miyajima, and A. Yamada, "Bandgap tuning of silicon nanowire arrays for application to all-silicon tandem solar cells," *Japanese Journal of Applied Physics,* vol. 56, no. 4S, p. 04CS03, 2017/02/10 2017, doi: 10.7567/jjap.56.04cs03.

[50] I. M. Asuo *et al.*, "High-performance pseudo-halide perovskite nanowire networks for stable and fast-response photodetector," *Nano Energy,* vol. 51, pp. 324-332, 2018/09/01/ 2018, doi: https://doi.org/10.1016/j.nanoen.2018.06.057.

[51] X. Zhang, X. Han, J. Su, Q. Zhang, and Y. Gao, "Well vertically aligned ZnO nanowire arrays with an ultra-fast recovery time for UV photodetector," *Applied Physics A,* vol. 107, no. 2, pp. 255-260, 2012/05/01 2012, doi: 10.1007/s00339-012-6886-6.

[52] D. Gedamu *et al.*, "Rapid Fabrication Technique for Interpenetrated ZnO Nanotetrapod Networks for Fast UV Sensors," *Advanced Materials,* vol. 26, no. 10, pp. 1541-1550, 2014, doi: https://doi.org/10.1002/adma.201304363.

[53] A. M. Selman and Z. Hassan, "Highly sensitive fast-response UV photodiode fabricated from rutile TiO2 nanorod array on silicon substrate," *Sensors and Actuators A: Physical,* vol. 221, pp. 15-21, 2015/01/01/ 2015, doi: https://doi.org/10.1016/j.sna.2014.10.041.

[54] Z. S. Hosseini, M. Shasti, S. R. Sani, and A. Mortezaali, "Photo-detector diode based on thermally oxidized TiO2 nanostructures/p-Si heterojunction," *Journal of Applied Physics,* vol. 119, no. 1, p. 014503, 2016, doi: 10.1063/1.4937546.

[55] D. Banerjee, C. Trudeau, L. F. Gerlein, and S. G. Cloutier, "Phonon processes in vertically aligned silicon nanowire arrays produced by low-cost all-solution galvanic displacement method," *Applied Physics Letters,* vol. 108, no. 11, p. 113109, 2016, doi: 10.1063/1.4944334.

[56] C. Carraro, R. Maboudian, and L. Magagnin, "Metallization and nanostructuring of semiconductor surfaces by galvanic displacement processes," *Surface Science Reports,* vol. 62, no. 12, pp. 499-525, 2007/12/31/ 2007, doi: http://dx.doi.org/10.1016/j.surfrep.2007.08.002.

[57] I. M. Asuo *et al.*, "Highly Efficient and Ultrasensitive Large-Area Flexible Photodetector Based on Perovskite Nanowires," *Small,* vol. 15, no. 1, p. 1804150, 2019, doi: https://doi.org/10.1002/smll.201804150.